ACS Catalysis

Letter

pubs.acs.org/acscatalysis

Redox-Controlled Crotyl Alcohol Selective Oxidation: In Situ Oxidation and Reduction Dynamics of Catalytic Pd Nanoparticles via Synchronous XANES/MS

Christine V. Gaskell,[†] Christopher M. A. Parlett,[†] Mark A. Newton,[‡] Karen Wilson,[†] and Adam F. Lee*[,†]

[†]Cardiff Catalysis Institute, School of Chemistry, Cardiff University, Cardiff CF10 3AT, U.K.

[‡]European Synchrotron Radiation Facility, 6 Rue Jules Horowitz, BP-220 Grenoble, F-38043, France

Supporting Information

ABSTRACT: In-situ, synchronous MS/XANES reveals the Pd catalyzed selective aerobic oxidation of crotyl alcohol is regulated by the balance between the oxidation state and reducibility. Dynamic XANES measurements provide a new, rapid method to determine redox kinetics of nanoparticles and identify important parameters to optimize catalyst design.

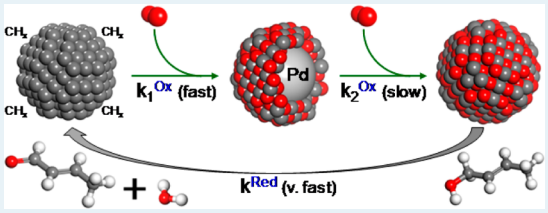

KEYWORDS: *palladium, alcohol, selective oxidation, XAS, kinetics*

INTRODUCTION

Pd nanoparticles (NPs) are ubiquitous in heterogeneous catalysis, effecting important technological transformations such as methane combustion for power generation, low-temperature CO oxidation in automotive catalytic converters, selective hydrogenation to purify monomer feedstocks, and diverse cross-couplings. Supported palladium are also promising catalysts for the selective oxidation (selox) of diverse substrates, including alcohols and carbohydrates (and even hydrogen).[1,2] Such selox chemistry represents an attractive route to the direct synthesis of high-value chemical intermediates utilized across the fine chemical, pharmaceutical, and agrochemical sectors. Significant recent progress has been made in developing Au,[3] Pd,[4] and AuPd[5,6] bimetallic NPs that are able to selectively oxidize primary and secondary saturated and allylic alcohols to their aldehyde and ketone counterparts, and even deactivated aromatics,[7] under environmentally benign reaction conditions. The discovery of new active and selective catalyst formulations and the importance of appropriate support selection and pretreatment has been accompanied by advances in our mechanistic understanding of such chemistry[8,9] and the oxidation state of the active site.[10]

We recently demonstrated that electron-deficient Pd^{2+} species at the surface of oxide-supported clusters or polymer-stabilized nanoparticles catalyze the heterogeneous liquid[4,11] and vapor phase oxidative dehydrogenation of allylic alcohols;[12] however, the stability of such sites and, indeed, redox properties of palladium surfaces and nanoparticles under catalytically relevant pressure regimes remain poorly understood. Recent vacuum and low-pressure studies of low-index Pd single crystals,[13−18] and Pd NPs deposited on Fe_3O_4 or SiO_x model films[19−22] support earlier literature indicating that palladium oxidation proceeds via fast oxygen dissociation and surface oxide formation, followed by slower diffusion through this passivating PdO selvedge and associated bulk oxide genesis.[23−25]

In this Letter, we exploit the powerful combination of energy-dispersive X-ray absorption spectroscopy (XAS) and online mass spectrometry (MS) to explore the redox chemistry of size- and shape-selected Pd nanoparticles in situ during the vapor phase selox of CrOH ($CH_3CH{=}CH{-}CHOH$) and relate this to their associated catalysis. This approach enables real-time quantification of the palladium oxidation state under dynamic conditions, enabling redox and oxygen diffusion kinetics to be extracted in the absence of solution phase diffusion limitations or competitive solvent effects present during liquid phase selox, while simultaneously quantifying catalytic activity/selectivity.

RESULTS AND DISCUSSION

A range of mesoporous silica- and alumina-supported Pd catalysts were prepared via incipient wetness impregnation,[4,26] or sol-immobilization of shape-selected nanoicosahedra[27] or nanorods[28] and exposed to alternating CrOH or O_2 pulses (~0.01 Hz) within a purpose-built in situ reaction cell.[29] Transmission energy dispersive X-ray absorption spectra were acquired every 750 ms at the Pd K-edge (24.35 keV) on ID24 of the ESRF, as described in the Supporting Information, with background-subtracted, normalized XANES spectra fitted to Pd foil and PdO standards to quantify their PdO content. Illustrative EXAFS spectra and XANES fits are provided in the Supporting Information. Catalyst samples were held

Special Issue: Operando and In Situ Studies of Catalysis

Received: July 5, 2012
Revised: August 8, 2012
Published: September 17, 2012

isothermally at temperatures between 80 and 250 °C and fed either crotyl alcohol (0.4 mmol min^{-1}) or O_2 (5 mmol min^{-1}) in a He carrier flow. Desorption products were detected by online QMS and quantified via careful background subtractions to remove ionization artifacts and corrected for molecular sensitivity factors. In all cases, net mass balances averaged across three alternating CrOH/O_2 cycles were >95%. Figure 1

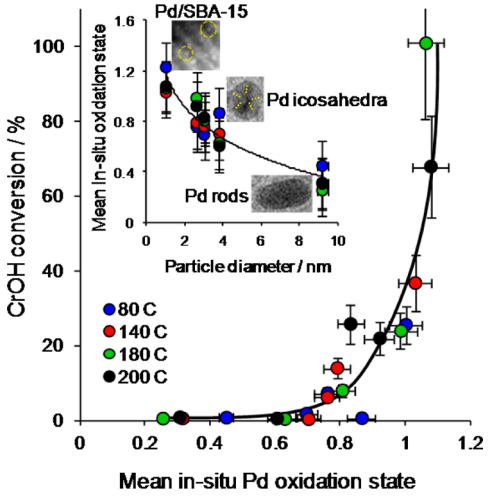

Figure 1. Surface area-normalized activity versus in situ oxidation state of size- and shape-selected Pd nanoparticles toward vapor phase CrOH selox; inset shows dependence of oxidation state on particle size.

illustrates the resulting global relationship between the Pd oxidation state (determined in situ and averaged across five oxidizing and reducing cycles) and the corresponding activity toward crotyl alcohol-selective oxidation. This establishes for the first time, in accordance with ex-situ XPS and XANES predictions,[10,26] that palladium-catalyzed crotyl alcohol oxidation is controlled by the concentration of Pd^{2+} centers, *irrespective of associated nanoparticle size or shape or oxide support type*. The temperature dependent activity and selectivity of the 2 wt % Pd/*m*-Al_2O_3 is detailed in the Supporting Information, alongside reaction rates and turnover frequencies for all catalysts at 80 °C, which show generally good agreement with their corresponding values from liquid phase CrOH selox in stirred batch reactors under static air, establishing a close link and relevance between the present dynamic vapor phase study and previous steady state literature.

To understand the flexible response of Pd nanoparticles to temperature and oxidizing/reducing conditions that we recently discovered during CrOH selox,[12] the redox kinetics (and capacity) of the diverse catalysts featured in Figure 1 have been analyzed isothermally at reaction bed temperatures from 80 to 200 °C. Figure 2 illustrates the catalyst redox behavior derived from Pd K-edge XANES linear combination fitting during a typical switching cycle from a CrOH to O_2 feed at 200 °C. The first striking observation is the synchronicity of Pd oxidation and reduction processes, whose temporal response appears independent of particle size or initial oxidation state across these nanoparticles. An exception is the 10 nm Pd nanorods (the largest particles in our study by a significant margin), which proved resistant to redox cycling under the reactant partial pressures and temperatures utilized, despite surface phase diagrams favoring Pd(111), (100), and (110) oxidation under such conditions[13,14,16,17] (the latter two facets dominat-

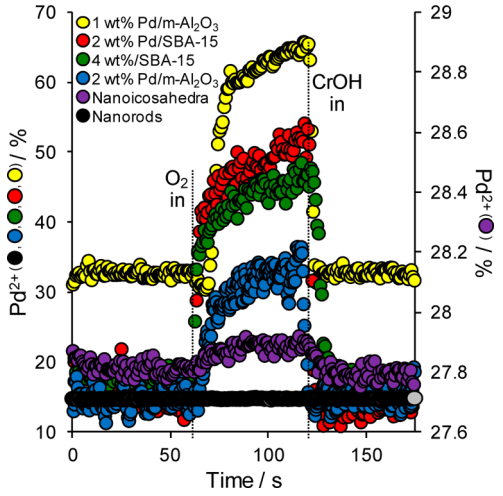

Figure 2. Pd nanoparticle redox response (from XANES) under CrOH/O_2 cycling at 200 °C.

ing the surface of nanorods[28]), evidencing a high kinetic barrier to oxygen incorporation at the short time scales employed. The redox process is fully reversible for over 5 cycles, with a complete return to the initial oxidation state attained on switching from CrOH to O_2 and back; note that such redox cycling was observed only at >140 °C. Another common feature is the apparent nonlinear oxidation process, which proceeds via rapid oxide formation, followed by a slower, more gradual oxidation step without reaching a plateau throughout the remaining oxidation cycle. In contrast, reduction occurs in a single, rapid step. Our observation that crotyl alcohol is able to reduce palladium oxide (coincident with the formation of adsorbed crotonaldehyde[12]), demonstrates that *in the absence of gas phase oxygen*, allylic alcohol selox occurs through a Mars–van Krevelen mechanism,[30] as proposed for methane combustion.[31]

To better understand the oxidation kinetics of the redox active NPs, their correspondence to a Mott–Cabrera model of rapid surface oxidation to form a *subsurface oxide* (adopting the terminology employed in single crystal studies[13]) and subsequent slow penetration of oxygen through this passivating layer and associated three-dimensional *bulk PdO* formation as a thin film was evaluated.[32,33] Figure 3 shows that excellent agreement with the resulting linear fits for all supported NPs at 200 °C was obtained, confirming the existence of two distinct oxidation regimes, occurring with over an order of magnitude difference in rates (Table 1): parabolic rate constants drop from k_{ox}^{1} = 40–136 $\mu mol^2\ s^{-1}$ during the initial oxidation step I, to $k_{ox}^{2} \leq 5\ \mu mol^2\ s^{-1}$ in the second step II. The analogous reduction process proceeded significantly faster than oxidation and in a single step, with a common rate constant of 220 ± 27 $\mu mol^2\ s^{-1}$ at 200 °C, suggesting that oxygen abstraction from the selvedge of our nanoparticles by CrOH is more facile than its incorporation. Our observation that bulk PdO appears to reduce directly back to Pd metal without intermediate *subsurface oxide* formation, mirrors in situ XPS measurements on the oxidation/reduction of Pd(111) by Ketteler and co-workers,[13] who inferred this *subsurface oxide* phase is, hence, metastable but forms an order of magnitude faster than corresponding bulk PdO, which is consistent with our rate data for nanoparticulate palladium.

Previous spectroscopic studies on palladium single crystal studies and thermogravimetric analyses on micrometer-sized Pd

dx.doi.org/10.1021/cs300445y | *ACS Catal.* 2012, 2, 2242–2246

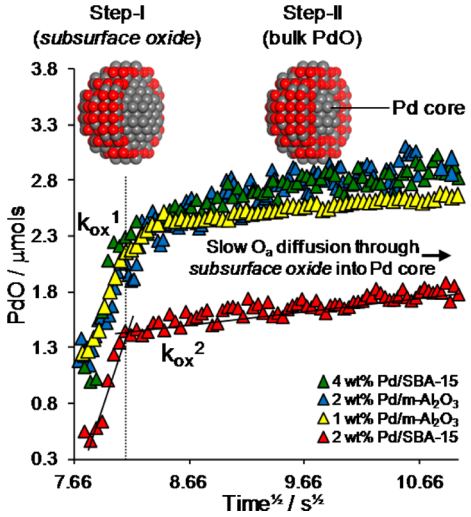

Figure 3. Correspondence to Mott–Cabrera diffusion-controlled oxidation of supported Pd NPs at 200 °C.

Table 1. Parabolic Rate Constants[a] for Pd NP Redox Processes at 200 °C

catalyst	k_{ox}^1/μmol^2 s^{-1}	k_{ox}^2/μmol^2 s^{-1}	k_{red}/μmol^2 s^{-1}
1 wt % Pd/*m*-Al_2O_3	61	4.6	195
2.2 wt % Pd/*m*-Al_2O_3	48	5.2	193
2.4 wt % Pd/SBA-15	41	0.6	238
4.1 wt % Pd/SBA-15	136	0.7	228

[a]Derived from Figure 3 assuming parabolic rate law [PdO] = $(2kt)^{1/2}$

powders have also reported significant differences in the activation energies for step I versus step II, with values ranges of 60–106 kJmol^{-1} for the former[13,14,23,25,34] and 110–180 kJmol^{-1} for bulk PdO formation determined at temperatures spanning 200–800 °C.[13,14,25,35] This difference has been ascribed to epitaxial growth of *subsurface oxide* over the underlying metal substrate, whose formation therefore requires relatively minor restructuring in comparison with that necessary for the subsequent phase transition to thermodynamically stable bulk PdO.[13]

Figure 4 reveals that *subsurface oxide* formation over sub-5 nm palladium nanoparticles likewise proceeds with a lower activation barrier than that for the genesis of PdO, despite significant differences in particle size/morphology, reaction temperature, and oxygen partial pressure employed in the present study compared with the preceding model systems, albeit with an energy difference of only 4–14 kJmol^{-1}. The absolute activation energies for step I oxidation of the 1 wt % Pd/m-Al_2O_3 and 2 wt % Pd/SBA-15 catalysts of around 110 kJmol^{-1} are close to those reported for polycrystalline Pd foils at similar low temperatures (106 kJmol^{-1})[25] and employed to model the redox chemistry of 5 wt % Pd/γ-Al_2O_3 catalysts (90 kJmol^{-1}).[36] Recent calculations suggest a barrier for O penetration into the Pd(111) surface of ∼150 kJmol^{-1}, far greater than any experimentally reported.[37]

Figure 4 also highlights a monotonic decrease in redox activation energies with nanoparticle size, being most facile for the 4% wt % Pd/SBA-15 sample for which oxidation requires only approximately 50 kJmol^{-1}. Interestingly, Au-Yeung et al. reported a similar decrease in the apparent activation energy for oxygen exchange into zirconia-supported PdO nanoparticles,[34] which fell from ∼128 to 64 kJmol^{-1} with increasing metal

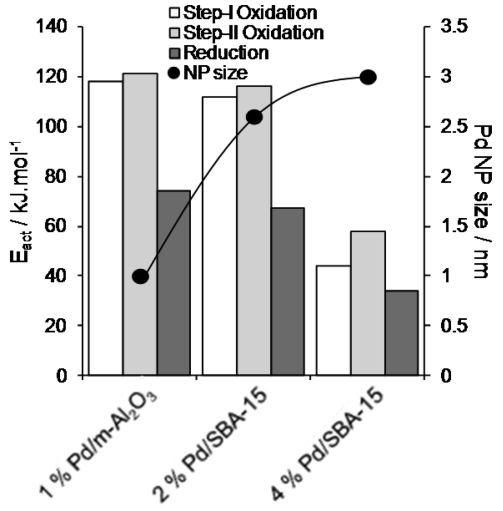

Figure 4. Apparent activation energies for oxidation and reduction of supported palladium nanoparticles (determined between 120 and 200 °C) as a function of particle size.

loading from 1.5 to 10 wt %. The origin of this phenomenon remains unclear, but has been attributed to weakening of the Pd–O bond with increasing PdO domain size[38] and may also reflect the smaller atomic displacements necessary to accommodate and transport oxygen within larger particles and, thus, lower strain induced during the initial stages of restructuring between metal and oxide.

There are few reports of activation energies for palladium oxide reduction, with Ketteler and co-workers reporting 140 kJmol^{-1} for the "reduction" of a bulk PdO adlayer over Pd(111) via lowering the oxygen background pressure from 0.35 to 3 × 10^{-3} Torr,[13] whereas Munir and Coombs report 208 kJmol^{-1} for the in vacuo "reduction" of microsized Pd powders.[23] Both values are significantly higher than those obtained for our palladium nanoparticles via direct chemical reduction of their PdO shells by crotyl alcohol, suggesting a very low barrier to C–H/O–H dissociation of the alcohol and the concomitant supply of surface hydrogen adatoms for oxygen abstraction from PdO (Mars–van Krevelen mechanism).

The relationship between palladium particle size and reducibility was further probed by calculating the redox capacity, defined as the change in XAS absorbance at 24.362 keV on switching between O_2 and CrOH feeds (Δ) relative to that between pure Pd metal and PdO phases (Δ_{max}), as a function of temperature. An inverse relation between particle size and redox capacity was observed for all nanoparticles (Figure 5) that exhibited redox chemistry, that is, those ≤3 nm, with redox capacity also displaying a quadratic temperature dependence. In other words, the stability of palladium metal (oxide) nanoparticles toward oxidation (reduction) increased with particle size, but decreased with temperature.

In light of our previous studies (and the results of Figure 1) suggesting that palladium oxide is the active phase in crotyl alcohol selox to crotonaldehyde, we anticipated that the redox capacity of dispersed metal nanoparticles, that is, their tendency to switch oxidation states in response to changing reaction conditions, could serve as a simple predictor of their catalytic performance. This hypothesis was tested by plotting crotonaldehyde selectivity as a function of redox capacity for the five Pd/*m*-Al_2O_3, Pd/SBA-15, and Pd-nanoicosahedra/*m*-

dx.doi.org/10.1021/cs300445y | ACS Catal. 2012, 2, 2242–2246

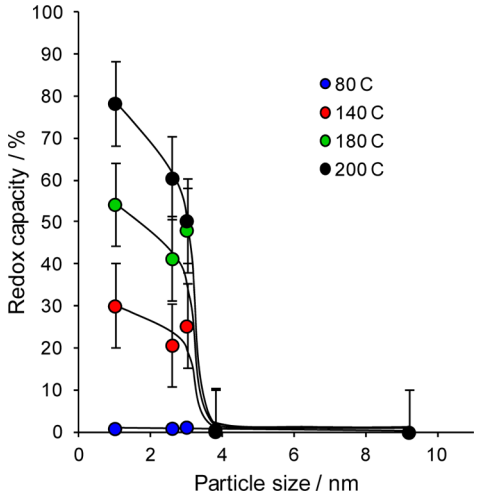

Figure 5. Redox capacity of supported palladium nanoparticles as a function of particle size.

Al_2O_3 catalysts employed in this study (the Pd nanorods were inactive), as shown in Figure 6. What emerges is a strong,

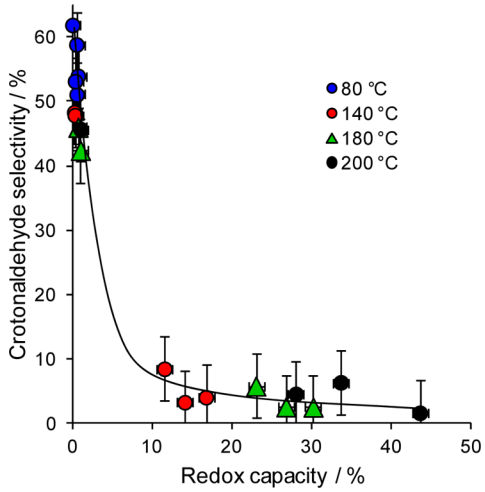

Figure 6. Crotonaldehyde selectivity versus redox capacity of supported palladium nanoparticles.

nonlinear, inverse correlation between redox capacity at any given reaction temperature and the resulting selective oxidative dehydrogenation of crotyl alcohol to crotonaldehyde. We interpret this by considering the redox capacity as a measure of the ease of in situ reduction of palladium oxide present in our supported nanoparticles; readily reducible nanoparticles will tend to exist in metallic form unless a high oxygen:alcohol reactant composition is maintained, favoring crotonaldehyde decarbonylation to CO and propene. Combining the results of Figure 1 and Figure 6, optimum crotonaldehyde yield is thus predicted for highly oxidized palladium nanoparticles that possess good stability toward thermal and chemical reduction at temperatures of ≥140 °C.

In conclusion, the redox behavior and corresponding catalytic performance of diverse Pd nanoparticles has been explored in situ by synchronous XAS and mass-spectrometry. Dynamic cycling of the catalyst environment between oxygen and crotyl alcohol permits rapid measurement of redox kinetics under conditions pertinent to the practical vapor phase-selective aerobic oxidation of crotyl alcohol to crotonaldehyde, and this methodology should be widely applicable to study redox processes within a host of catalytic oxidations. Oxidation of palladium nanoparticles followed Mott−Cabrera kinetics under our conditions, with rapid formation of a subsurface oxide overlayer preceding slower diffusion-controlled bulk PdO formation. Crotyl alcohol conversion was proportional to the concentration of palladium oxide in situ, whereas selectivity to crotonaldehyde was determined by the associated oxide reducibility. Temperature-programmed reduction and reoxidation measurements to measure oxide content and thermochemical stability, could thus provide a simple laboratory-based tool to screen for promising nanoparticulate palladium selox catalysts.

■ ASSOCIATED CONTENT

Ⓢ Supporting Information

Full catalyst synthesis, electron microscopy and reaction conditions, and illustrative EXAFS spectra and XANES fits. This material is available free of charge via the Internet at http://pubs.acs.org.

■ AUTHOR INFORMATION

Corresponding Author

*Phone: +44 2920 874778. E-mail: leeaf@cardiff.ac.uk.

Notes

The authors declare no competing financial interest.

■ ACKNOWLEDGMENTS

We thank the EPSRC (EP/E046754/1; EP/G007594/2) for financial support, access to electron microscopy facilities, and a Leadership Fellowship (AFL) and studentship support (C.V.G. and C.M.A.P.); and the ESRF for beamtime (CH2432). We gratefully acknowledge the assistance of Dr. Nicole Hondow (University of Leeds) and Dr. Teck Lim (University of Oxford) with TEM image acquisition.

■ REFERENCES

(1) Vinod, C. P.; Wilson, K.; Lee, A. F. *J. Chem. Technol. Biotechnol.* **2011**, *86* (2), 161−171.
(2) Dimitratos, N.; Lopez-Sanchez, J. A.; Hutchings, G. J. *Chem. Sci.* **2012**, *3* (1), 20−44.
(3) Della Pina, C.; Falletta, E.; Prati, L.; Rossi, M. *Chem. Soc. Rev.* **2008**, *37* (9), 2077−2095.
(4) Hackett, S. E. J.; Brydson, R. M.; Gass, M. H.; Harvey, I.; Newman, A. D.; Wilson, K.; Lee, A. F. *Angew. Chem., Int. Ed.* **2007**, *46* (45), 8593−8596.
(5) Enache, D. I.; Edwards, J. K.; Landon, P.; Solsona-Espriu, B.; Carley, A. F.; Herzing, A. A.; Watanabe, M.; Kiely, C. J.; Knight, D. W.; Hutchings, G. J. *Science* **2006**, *311* (5759), 362−365.
(6) Lee, A. F.; Ellis, C. V.; Wilson, K.; Hondow, N. S. *Catal. Today* **2010**, *157* (1−4), 243−249.
(7) Kesavan, L.; Tiruvalam, R.; Rahim, M. H. A.; bin Saiman, M. I.; Enache, D. I.; Jenkins, R. L.; Dimitratos, N.; Lopez-Sanchez, J. A.; Taylor, S. H.; Knight, D. W.; Kiely, C. J.; Hutchings, G. J. *Science* **2011**, *331* (6014), 195−199.
(8) Lee, A. F.; Chang, Z.; Ellis, P.; Hackett, S. F. J.; Wilson, K. *J. Phys. Chem. C* **2007**, *111* (51), 18844−18847.
(9) Naughton, J.; Pratt, A.; Woffinden, C. W.; Eames, C.; Tear, S. P.; Thompson, S. M.; Lee, A. F.; Wilson, K. *J. Phys. Chem. C* **2011**, *115* (51), 25290−25297.
(10) Lee, A. F.; Hackett, S. F. J.; Hargreaves, J. S. J.; Wilson, K. *Green Chem.* **2006**, *8* (6), 549−555.
(11) Lee, A. F.; Wilson, K. *Green Chem.* **2004**, *6* (1), 37−42.

(12) Lee, A. F.; Ellis, C. V.; Naughton, J. N.; Newton, M. A.; Parlett, C. M. A.; Wilson, K. *J. Am. Chem. Soc.* **2011**, *133* (15), 5724−5727.
(13) Ketteler, G.; Ogletree, D. F.; Bluhm, H.; Liu, H.; Hebenstreit, E. L. D.; Salmeron, M. *J. Am. Chem. Soc.* **2005**, *127* (51), 18269−18273.
(14) Han, J. Y.; Zemlyanov, D. Y.; Ribeiro, F. H. *Surf. Sci.* **2006**, *600* (13), 2752−2761.
(15) Zemlyanov, D.; Aszalos-Kiss, B.; Kleimenov, E.; Teschner, D.; Zafeiratos, S.; Havecker, M.; Knop-Gericke, A.; Schlogl, R.; Gabasch, H.; Unterberger, W.; Hayek, K.; Koltzer, B. *Surf. Sci.* **2006**, *600* (5), 983−994.
(16) Gabasch, H.; Unterberger, W.; Hayek, K.; Klotzer, B.; Kleimenov, E.; Teschner, D.; Zafeiratos, S.; Havecker, M.; Knop-Gericke, A.; Schlogl, R.; Han, J. Y.; Ribeiro, F. H.; Aszalos-Kiss, B.; Curtin, T.; Zemlyanov, D. *Surf. Sci.* **2006**, *600* (15), 2980−2989.
(17) Salmeron, M.; Schlögl, R. *Surf. Sci. Rep.* **2008**, *63* (4), 169−199.
(18) Kan, H. H.; Weaver, J. F. *Surf. Sci.* **2009**, *603* (17), 2671−2682.
(19) Schalow, T.; Brandt, B.; Starr, D. E.; Laurin, M.; Shaikhutdinov, S. K.; Schauermann, S.; Libuda, J.; Freund, H.-J. *Angew. Chem., Int. Ed.* **2006**, *45* (22), 3693−3697.
(20) Schalow, T.; Brandt, B.; Starr, D. E.; Laurin, M.; Shaikhutdinov, S. K.; Schauermann, S.; Libuda, J.; Freund, H. J. *Phys. Chem. Chem. Phys.* **2007**, *9* (11), 1347−1361.
(21) Brandt, B.; Schalow, T.; Laurin, M.; Schauermann, S.; Libuda, J.; Freund, H. J. *J. Phys. Chem. C* **2007**, *111* (2), 938−949.
(22) Westerstrom, R.; Messing, M. E.; Blomberg, S.; Hellman, A.; Grönbeck, H.; Gustafson, J.; Martin, N. M.; Balmes, O.; van Rijn, R.; Andersen, J. N.; Deppert, K.; Bluhm, H.; Liu, Z.; Grass, M. E.; Hävecker, M.; Lundgren, E. *Phys. Rev. B* **2011**, *83* (11), 115440.
(23) Munir, Z. A.; Coombs, P. G. *Metall. Trans. B* **1983**, *14* (1), 95−99.
(24) Su, S. C.; Carstens, J. N.; Bell, A. T. *J. Catal.* **1998**, *176* (1), 125−135.
(25) Veser, G.; Wright, A.; Caretta, R. *Catal. Lett.* **1999**, *58* (4), 199−206.
(26) Parlett, C. M. A.; Bruce, D. W.; Hondow, N. S.; Lee, A. F.; Wilson, K. *ACS Catalysis* **2011**, *1* (6), 636−640.
(27) Xiong, Y.; McLellan, J. M.; Yin, Y.; Xia, Y. *Angew. Chem.* **2007**, *119* (5), 804−808.
(28) Xiong, Y.; Cai, H.; Wiley, B. J.; Wang, J.; Kim, M. J.; Xia, Y. *J. Am. Chem. Soc.* **2007**, *129* (12), 3665−3675.
(29) Newton, M. A. *Top. Catal.* **2009**, *52* (10), 1410−1424.
(30) Doornkamp, C.; Ponec, V. *J. Mol. Catal. A: Chem.* **2000**, *162* (12), 19−32.
(31) Müller, C. A.; Maciejewski, M.; Koeppel, R. A.; Baiker, A. *J. Catal.* **1997**, *166* (1), 36−43.
(32) Cabrera, N.; Mott, N. F. *Rep. Prog. Phys.* **1949**, *12* (1), 163.
(33) Atkinson, A. *Rev. Mod. Phys.* **1985**, *57* (2), 437−470.
(34) Au-Yeung, J.; Bell, A. T.; Iglesia, E. *J. Catal.* **1999**, *185* (1), 213−218.
(35) Shimada, E.; Yamashita, H.; Matsumoto, S.; Ikuma, Y.; Ichimura, H. *J. Mater. Sci.* **1999**, *34* (16), 4011−4015.
(36) Wolf, M. M.; Zhu, H.; Green, W. H.; Jackson, G. S. *Appl. Catal., A* **2003**, *244* (2), 323−340.
(37) German, E. D.; Sheintuch, M.; Kuznetsov, A. M. *J. Phys. Chem. C* **2009**, *113* (34), 15326−15336.
(38) Chou, P.; Vannice, M. A. *J. Catal.* **1987**, *105* (2), 342−351.